AIAA JOURNAL
Vol. 32, No. 8, August 1994

Atomization Experiments in a Coaxial Coflowing Mach 1.5 Flow

Kakkattukuzhy Issac,* Azzedine Missoum,† James Drallmeier,‡ and Andrew Johnston†
University of Missouri—Rolla, Rolla, Missouri 65401

Extensive flow visualization using schlieren/shadowgraph, flash photography and short duration (ns) laser imaging, and drop size measurements are reported in this work. The supersonic nozzle operating conditions ranged from an overexpanded to highly underexpanded mode. A phenomenon of the liquid jet expanding into a bubblelike formation as it interacts with the first set of waves is explained. Photographic evidence indicated the presence of a primary region enclosed by the first shock cell where the primary breakup occurred, a secondary region enclosing the bubblelike formation, and a third subsonic region further downstream. Atomization seemed to be initiated by the growth of three-dimensional structures on the liquid surface. Subsequent detachment of the three-dimensional structure as fine droplets by the intense shear at the liquid-gas interface was observed. This seems to partially confirm the boundary-layer stripping mechanism proposed by Taylor and Ranger and Nicholls.

Nomenclature

A = area, m^2
c_f = skin friction coefficient
D = exit diameter, m
D_{32} = Sauter mean diameter, m, $\int_0^\infty n(D)D^3 dD / \int_0^\infty n(D)D^2 dD$
d = drop diameter, m
l = circumference, m
$\dot{m}$ = mass flow rate, kgs^{-1}
p = pressure, Nm^{-2}
R = exit radius, m
Re = Reynolds number, $\rho UD/\mu$
r = radial coordinate
S = surface area, m^2
U = velocity at $x = 0$, ms^{-1}
u = velocity, ms^{-1}
u_l = drop velocity, ms^{-1}
We = Weber number, $\rho_g U_g^2 d/\sigma$
x = axial coordinate
μ = dynamic viscosity, $kgm^{-1}s^{-1}$
ρ = density, kgm^{-3}
σ = surface tension, Nm^{-1}

Subscripts

amb = ambient
e = nozzle exit
g = gas
l = liquid
0 = stagnation condition

I. Introduction

THE atomization of liquid jets resulting from their sudden exposure to a high-velocity gas flow has many applications in the fields of aerospace engineering, energy utilization, and material synthesis. The rates of mixing and combustion in an engine can be greatly enhanced by virtue of better atomization of the fuel jet. In aerospace vehicles, such as the high-speed civil transport (HSCT) under development, atomization, mixing, and combustion must be accomplished within a short distance between the fuel injection port and the end of the combustion chamber. In vehicles such as the HSCT in which supersonic combustion ramjets (scramjets) are anticipated for propulsion, the aforementioned processes of spray formation, mixing, and combustion must take place at supersonic velocities that limit the time available for their efficient completion. Besides the desire for the highest efficiency, mounting environmental concerns dictate the design and development of environment-friendly systems. New fuels such as slurries and energetic fuels impose additional demands on the system because their properties are drastically different from those of conventional fuels. In material processing, metal powder production and metal coating by liquid dynamic compaction can be improved by using a high-velocity inert gas for atomizing the molten metal. Because of the inert surroundings and the rapidity of the process, metal oxidation takes place at low levels. Moreover, the rapidly expanding gas provides low temperatures for rapid solidification of the molten metal resulting in better crystal structure.

In spite of the availability of some commercial systems that use supersonic atomization, the processes involved are extremely complex and little understood. A supersonic flow has a highly variable property field that depends on the operating pressure ratio. In a Mach 1.5 flow, the gas static temperature drops by nearly a third (300 to 200 K) from the nozzle inlet to its exit. The molten metal in a supersonic atomizer may encounter a temperature variation of nearly 600 K during its passage through the atomization device. Over such a high temperature range, the liquid and the gas undergo large variations in properties such as viscosity, thermal conductivity, and surface tension. The two-phase flowfield itself starts with supersonic flow in the gas phase and incompressible flow in the liquid phase. It is obvious that analytical/computational/experimental studies of the process must consider multiphase flow, turbulence, heat transfer, solidification, vaporization, and many other phenomena.

Many aspects of droplet evaporation and combustion have been reviewed recently.[1] Previous experimental work on high-speed aerodynamic atomization can be roughly divided into three categories: 1) transverse injection in supersonic crossflow,[2–5] 2) shattering of liquid drops by a traversing shock,[6,7] and 3) subsonic coflow injection.[8–10] In a recent study,[11] the effect of shock waves on liquid atomization of a two-dimensional airblast atomizer in which the air and the liquid issued from slits and the air jet impinged the liquid jet at an angle was investigated. The flowfield in this work was very complex because of the angle between the air jet and the liquid jet. Aerodynamic atomization, emphasized in the present study, differs from conventional airblast atomization because the former avoids intricate injector designs and the atomization is caused mainly by the exposure of the liquid jet to the high-momentum gas flow. In addition, it differs from atomization by high-pres-

Received May 7, 1993; revision received March 16, 1994; accepted for publication March 18, 1994.

*Associate Professor of Aerospace Engineering, Mechanical and Aerospace Engineering and Engineering Mechanics Department. Member AIAA.

†Graduate Student, Mechanical and Aerospace Engineering and Engineering Mechanics Department. Student Member AIAA.

‡Assistant Professor, Mechanical and Aerospace Engineering and Engineering Mechanics Department. Senior Member AIAA.

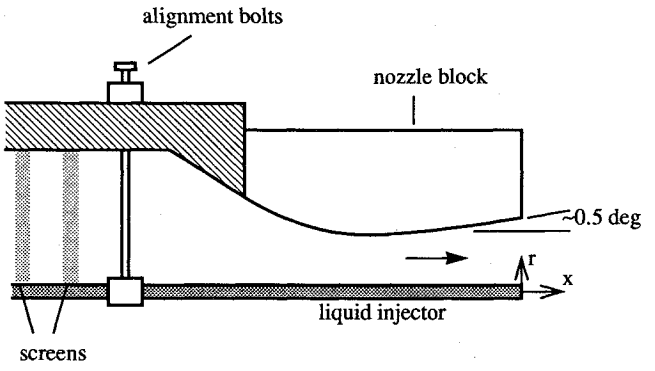

Fig. 1 Schematic diagram of the liquid injector.

sure injection[12] in that, in high-pressure atomizers, the liquid accelerates to very high velocities within the injector and emerges into the still gas medium in a highly agitated state (high turbulence). Cavitation can further complicate the state of the liquid at the injector exit.

In a supersonic flow with shock waves and expansion waves present, the pressure distribution is highly irregular. When the liquid surface encounters this uneven pressure distribution, it may deform as a precursor to its total breakup. Boundary-layer stripping, in which the shearing action exerted by the high-speed gas stream on the liquid surface leads to the formation of a boundary layer and subsequent surface stripping, has been proposed in earlier studies.[6,13]

In the following sections, we present the experimental part of our study on aerodynamic atomization in supersonic, coaxial systems. A complementary analytical work on the primary breakup of the jet is described in Ref. 14. The supersonic atomizer employed in our experiments and the associated instrumentation consisting of several types of flow visualization apparatus and a phase/Doppler particle analyzer (P/DPA) are briefly described in the next section. A more detailed description of the flow facility and instrumentation is given in Ref. 15. The thrust of this paper is on the overall characterization of the spray. The quantitative data are presented in the Sec. III.

II. Flow Facility and Instrumentation

The supersonic blowdown wind tunnel at the University of Missouri—Rolla can operate continuously over a wide range of Mach numbers. Compressed dry air from storage tanks (7.6 m^3) at 140 atm pressure is piped into the settling chamber where the pressure is reduced to ≤ 27 atm for safety reasons. The tunnel setup consists of a 1.25-m-long, 0.4-m-diam settling chamber fitted with a flow straightener and several fine screens. The 10-mm nominal diameter nozzle is shown in Fig. 1. A 6-mm-o.d. injector tube enters the settling chamber centrally at the back through airtight fittings. A positioning and support mechanism is used for accurate positioning and firm support of the liquid injector just before it enters the nozzle. The size of the injector tube is reduced to 1.8 mm o.d. (1.4 mm i.d.) before it enters the nozzle. The thickness of the liquid injector lip has been carefully machined down to nearly 0.1 mm to avoid any significant base flow at the injector tip. The injector tube was checked for vibration-free operation. A pressure transducer and a copper-constantan thermocouple are inserted at the end of the settling chamber to measure the stagnation pressure and the stagnation temperature, respectively. Softened city water is supplied from a pressurized tank whose injection pressure is measured at a pressure port about 15 cm (6 in.) upstream of the injector exit using a pressure transducer. The water flow rate was measured by a flow meter. Flow visualization was done using black and white schlieren and shadowgraph, using continuous light, and direct photography, using a strobe light. Additionally, the liquid jet was illuminated by a thin sheet of light from a frequency-doubled Nd:YAG pulsed laser (~8 ns) operating at a 532-nm (green) wavelength to record instantaneous images of the spray. A camera was placed perpendicular to the illuminated plane and the image recorded when the laser, operating in the single-pulse mode, emitted a light pulse when triggered by the camera shutter. An electronic timer was used to synchronize the camera shutter and the laser. Quantitative measurements were made using a P/DPA equipped with a fast Fourier transform (FFT) processor that facilitated high-speed flow measurements. The P/DPA technique is described in detail in Ref. 16. The P/DPA is equipped with an FFT (DSA 3000 series) processor. The Fourier analysis is an effective means of locating and quantifying the frequency and phase of a signal when it is immersed in background noise.

III. Results and Discussion

The first phase of the study consisted of characterizing the supersonic flow without liquid injection. Schlieren and shadowgraph pictures were taken under various lighting and magnification conditions. These pictures were then compared with those from Love et al.,[17] which showed similar flowfields for the same geometry and conditions of operation. The presence of the incident shock, the Mach disk, the slip lines, etc., were confirmed with the help of the schlieren/shadowgraph pictures. Shock/expansion angles and Mach number calculations[18,19] were also performed, and the wave angles agreed qualitatively with those in the schlieren/shadowgraph pictures.

Overexpanded/Underexpanded Operation

A Mach 1.5 nozzle was operated under different reservoir pressures ranging from 310 to 793 kPa (45 to 115 psia). The nozzle operated at design conditions (fully expanded flow) when the reservoir pressure was 372 kPa (54 psia). In the overexpanded mode of operation, an oblique shock wave emanates at the nozzle lip and extends toward the centerline. When operating the nozzle at reservoir pressures higher than the design pressure of 372 kPa (54 psia), the jet exit pressure is higher than the ambient or back pressure and the jet is underexpanded. The maximum reservoir pressure used in this set of experiments was 793 kPa (115 psia). The corresponding jet exit static pressure p_e was 216 kPa (31.3 psia), and the ambient pressure p_{amb} was atmospheric, 101.3 kPa (14.7 psia), which gives a maximum pressure ratio $p_e/p_{amb} = 2.1$.

For underexpanded operation, a shock wave was observed at the nozzle lip in addition to the expansion fan. This shock wave apparition at the nozzle lip can be explained by the following reasoning of Courant and Friedrichs.[20] The intercepting shock will be present even in the presence of liquid injection, and therefore it can be understood by referring to Fig. 2, which is a schematic diagram for the two-phase case. The flow continues uninfluenced by the state in the ambient (region 1) until it meets the first Mach line (ab) issuing from the nozzle lip (a), i.e., the inner border of the expansion fan. Owing to the divergence of the jet, the pressure decreases along the axis beyond the nozzle exit plane. Across the expansion fan, the pressure decreases to the ambient pressure at the nozzle lip and hence to below ambient pressure further out. In other words, the pressure is below p_{amb} at the outer border (ac) of the expansion fan, whereas it equals p_{amb} at the free jet boundary. Consequently, there is a pressure gradient acting from the jet boundary toward the interior of the jet. This pressure gradient makes the jet curve inward and results in an intercepting shock as observed in the present experiments.

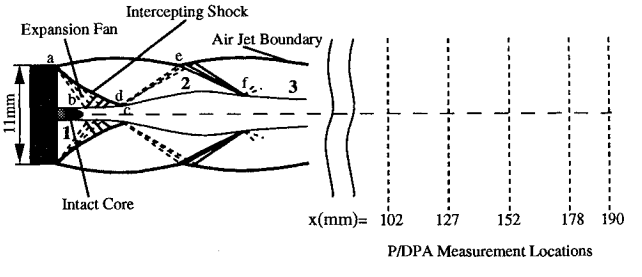

Fig. 2 Schematic diagram of the spray interacting with the surrounding gas flow.

Qualitative Spray Behavior in Supersonic Flow

The second phase of the study consisted of flowfield characterization with liquid injection. The air stagnation pressure and the liquid injection pressure were varied to obtain a range of conditions to investigate the effects of liquid flow rate, air stagnation pressure, and air-to-liquid mass flow ratio ($\dot{m}_g/\dot{m}_l$). The liquid injection flow rate was varied from 2.1 to 10. 5 ml/s (2 to 10 gal/h), which corresponds to a liquid phase Reynolds number (based on liquid injector diameter) range of 1750 to 9000. The fluid properties and the experimental conditions are given in Table 1. The airflow was at the following nominal conditions at the nozzle exit: Mach number = 1.5, velocity = 432 m/s (1419 fps), and temperature = 207 K (373°R). The gas phase Reynolds number (Re_{xg}) at the nozzle exit based on streamwise distance from the nozzle throat ranged from 1.27×10^6 to 3.24×10^6. For the design pressure, the gas phase boundary layer on the liquid tube wall at the exit was estimated to be ~0.5 mm thick. The nozzle back pressure was 1 atm for all cases. The liquid temperature shown in Table 1 was measured in the pressurized tank, while the liquid static pressure shown was estimated at the injector exit using the calibration curve described in the following paragraph. At the injector exit, the temperature was lower because of cooling by the low-temperature external airflow. The air-to-liquid mass flow ratio varied from 5 to 70. These simulated conditions differ from a real engine's operating conditions mainly in the gas temperature. In a scramjet engine, the temperature at the combustor inlet would be ~1000 K compared with ~200 K in the present simulation. The air-to-liquid mass flow ratio in a hydrocarbon-fueled engine would be ~50, which falls within the range considered in the present work.

The liquid injector exit pressure is an important parameter necessary to characterize the flow with liquid injection. Because of the small size of the injector, it was not practical to use a probe to measure the liquid static pressure at the injector tip. Instead, the liquid static pressure was measured about 15 cm upstream of the injector tip. A calibration curve (see Ref. 15) was prepared by plotting the pressure drop as a function of the dynamic pressure for various values of the liquid flow rate. A linear least-squares fit represented the calibration data fairly accurately. This calibration curve can be used to determine the injector exit pressure in the presence of the enveloping supersonic flow by measuring the liquid flow rate and the pressure at the liquid pressure port.

Shock-expansion calculations[18,19] were also performed for these cases with liquid injection. This simple approach for qualitative comparison with the experimentally observed wave pattern is justified because of the small divergence angle of the nozzle (≈1 deg).

Table 1 Experimental conditions

	T, K	p, kPa	μ, kgm^{-1}s^{-1}	q, Nm^{-1}
Air (reservoir)	300	310–793	18.2×10^{-6}	—
Water	293	90–207	1.1×10^{-3}	0.0735

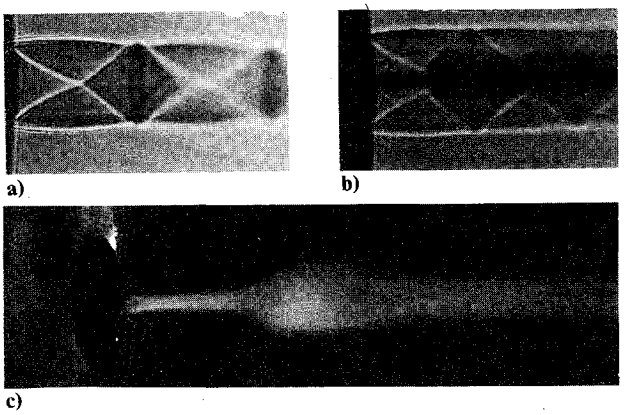

Fig. 3 Time-averaged flow visualization pictures: a) shadowgraph of the gas flow without liquid jet, b) shadowgraph of the liquid jet interacting with the gas flow, and c) flash photograph of the liquid jet interacting with the gas flow.

Interestingly, these calculations showed that using the liquid jet boundary as a free jet (constant pressure) boundary enabled the shock-expansion theory to give a fairly accurate representation of the wave angles and, as will be seen, the visible boundary of the liquid jet in the first two shock cells. Obviously, since the spray boundary is deflected by the waves, a "solid wall" boundary condition would not be appropriate in this case. Further downstream, where viscous effects overwhelm the sharp wave boundaries, the shock-expansion theory becomes inadequate. It clearly indicates the usefulness of adopting Euler/Navier-Stokes computational fluid dynamics techniques to simulate the flowfield in future studies.

The flow visualization studies reported in this paper focus only on the fully expanded and underexpanded operation. Figure 3a shows a shadowgraph of the gas flow only. Figure 3b shows a shadowgraph of the liquid/gas interaction, and Fig. 3c shows a picture of the spray illuminated with a strobe light. The shadowgraph pictures are time averaged because of the continuous light source used for illumination. When compared with the time scales of the gas phase flow, the direct photograph of the spray (Fig. 3c) taken with the strobe light may also be considered time averaged.

As the liquid jet progresses downstream, it interacts with the expansion fan/shock wave from the nozzle lip, which results in a sudden enlargement of the jet cross section into a bubblelike formation (Figs. 2 and 3c). The formation of the bubble can be explained, to a first approximation, using the principles of wave interaction with a constant pressure boundary. The liquid jet, having low velocities in the first shock cell, can be assumed to be incompressible. Therefore, any changes in pressure in the primary spray region can be approximated by Bernoulli's equation. However, these variations of the pressure in the central, subsonic region are small compared with those in the gas phase, which justifies the treatment of the spray boundary as a constant pressure boundary in the primary breakup region. Thus, as the expansion fan from the nozzle lip (point a in Fig. 2) reaches the spray, its boundary (bc) starts turning away from the axis in accordance with the law of wave reflection from a constant pressure boundary. On encountering the intercepting shock, the boundary turns in the opposite direction (toward the spray axis). The expansion fan from the nozzle lip will reflect as compression waves from the spray boundary coalescing into a shock as can be seen in Fig. 3b, whereas the intercepting shock reflects as an expansion fan toward the outer edge of the gas jet. Further reflection of these two sets of waves will take place at the boundary between the gas jet and the ambient air. Under the influence of these two sets of waves reflecting back and forth, the spray boundary further turns, finally making it nearly parallel to the gas flow. The spray assumes the bulbous shape seen in the flow visualization pictures, first by the outward and then by the inward turning of the spray-gas phase interface. The preceding scenario is rather simplistic but very useful. In reality, the wave interaction is much more complex, and many details, such as the expansion waves present at the nozzle exit due to the diverging, nonuniform flow from the nozzle, are not accounted for. These arguments are primarily applicable in the underexpanded regime because the overexpanded mode of nozzle operation was not investigated in detail. The strong interaction with the waves causing the spray to balloon into the bulbous shape can, most likely, be considered to be the critical process that completes the transformation of the liquid jet into a fine spray. Further interaction appears to be essentially a mixing process for the conditions investigated in the present experiments.

The relatively high pressures, low temperatures, and low velocities in the internal passages of the liquid injector are not likely to induce cavitation. Cavitation in the internal passages would have made the liquid jet unsteady and readily observable. No such unsteadiness was detected in the experiments. The minimum pressure in the shock cells of the external flow was ~75 kPa, abs, well above cavitation pressure ($p_v \approx 2.338$ kPa, abs at 20°C). Therefore, cavitation can be ruled out also in the wave-interaction region of the present experiments.

Primary Spray Evolution

Several features of the flowfield in the primary breakup region were revealed when examined with the help of a microscope and a

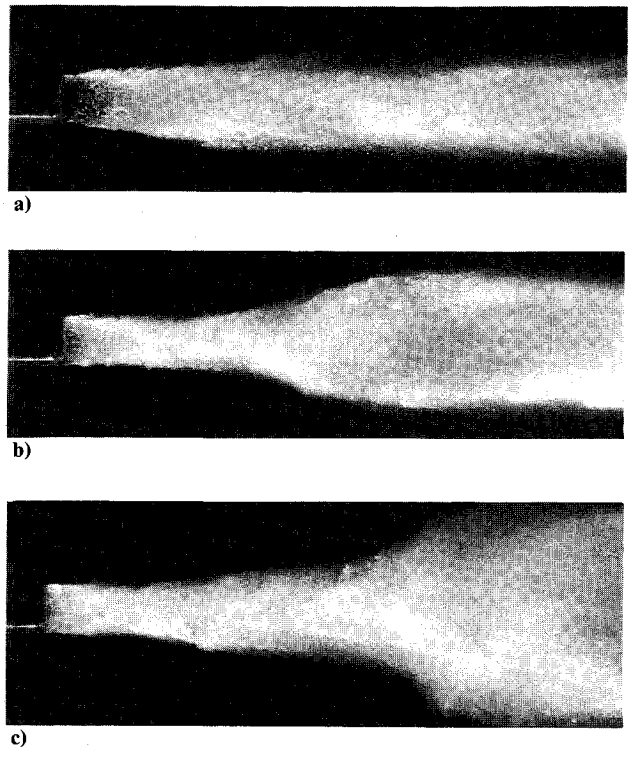

Fig. 4 Effect of increasing air dynamic pressure on the liquid jet, $\dot{m}_g/\dot{m}_l$ = 5 g/s: a) p_0 = 380 kPa, b) p_0 = 517 kPa, and c) p_0 = 793 kPa.

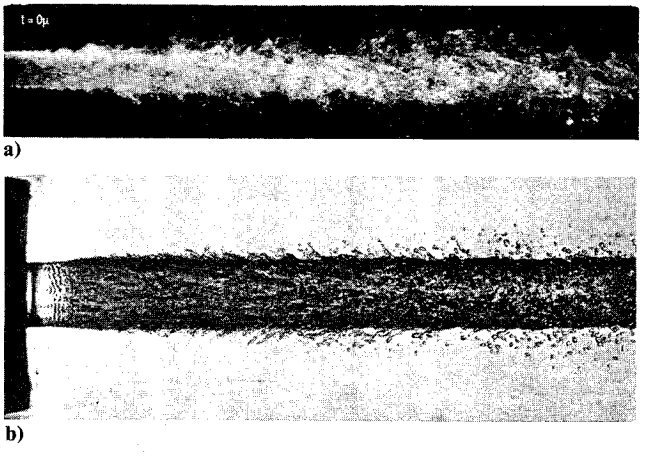

Fig. 5 Round liquid jet in subsonic coflowing airstream; a) D_l = 2 mm, U_l = 22 m/s, U_g = 155 m/s (from Mayer and Krulle[10]) and b) D_l = 6.4 mm, U_l = 25.3 m/s, U_g = 0.0 m/s (from Hoyt and Taylor[23]).

video system under various trial-and-error illumination setups. A similar setup with a high magnification 35-mm camera yielded the photographs with better resolution given in Fig. 4. This figure shows the primary breakup region for a constant liquid flow rate of 5 ml/s and three values of the air stagnation pressure (380, 517, and 793 kPa, abs). The airflow Reynolds numbers (Re_{xg}) based on streamwise distance from the nozzle throat were 1.53 × 10^6, 2.09 × 10^6, and 3.24 × 10^6 in Fig. 4 (a, b, and c, respectively). These photographs were taken using an 8-ns light pulse from the pulsed laser. Figure 4a corresponds to fully expanded flow, and Figs. 4b and 4c correspond to underexpanded flow. At the jet exit, the liquid jet boundary can be seen to deflect toward the axis as the air pressure increases (Fig. 4). This decrease in the initial spray angle is the result of the increasing pressure ratio p_{eg}/p_{el} that controls the deflection of the initial liquid jet boundary. The various subregions in the primary breakup region are indicated in the photographs of the jet structure given in Fig. 4. Photographs of the free surface wave structure, very similar to those given in Fig. 4, are also given in Refs. 10 and 21–23; two of which are reproduced in Fig. 5. A schematic diagram of the primary breakup region showing the three subregions is given in Fig. 6. The first subregion immediately at the jet exit, dark in the photographs (Fig. 4), which appeared glassy and smooth under direct viewing, is apparently still not broken up by the airflow. The smooth surface of this subregion is seen to diminish in size as the air pressure increases. A nearly conical intact core (Fig. 2), 1 to 2 injector tube diameters long, was also clearly visible under direct observation with backlighting and in the high magnification photographs. Following the glassy region, a three-dimensional structure develops on the liquid jet surface. In spite of the photographs in Figs. 4 and 5 originating from different labs, the main difference among them seems to be in the scale of the three-dimensional surface structure. Therefore, one is led to conclude that the features seen in Figs. 4 and 5 are not the result of any peculiarities associated with the respective experiments. It may be observed from the five photographs in Figs. 4 and 5 that the texture of the liquid surface structure becomes finer as the gas phase dynamic pressure increases, a behavior similar to the increase in the fineness of the turbulence structure with Reynolds number observed in laminar-to-turbulent transition studies.[21,22,24]

Jet disintegration via membrane-type ligaments is discussed in Ref. 9. In this mode, the round liquid jet is believed to transform into a thin liquid sheet, which develops Kelvin-Helmholtz waves and breaks up into drops. Kelvin-Helmholtz waves are essentially an inviscid phenomenon.[25] Tollmien-Schlichting (T-S) waves are, however, viscosity dominated.[26] The flow visualization photographs of Hoyt and Taylor[22,23] show primary waves similar to the T-S waves that break up into a three-dimensional structure. Van Dyke[24] gives additional examples of surface waves and suggests that they are T-S waves. The similar nature of the surface waves of the present work to those in Refs. 21–24, therefore, supports the inference that the waves in Fig. 4 are likely to be T-S waves. However, the primary axisymmetric instability waves do not appear to develop fully in the present case (Fig. 4) before their breakdown into the finer three-dimensional structure. The main difference in the experimental conditions of the present study from those of Refs. 21–23 is the much higher gas phase dynamic pressure of the present experiments. It is possible that, at higher gas phase dynamic pressure, the T-S waves do not fully develop before transition to a three-dimensional structure. These observations are not necessarily inconsistent with earlier studies[9] because the present work probably falls into an atomization regime different from that of Ref. 9 in which the gas phase dynamic pressure was much lower.

It has been pointed out that the nature of the gas boundary layer on the liquid injector tube outer surface may influence the behavior of the liquid jet.[27] The relative importance to the spray behavior of the level of turbulence in the liquid before its emergence from the injector tube and the state of the gas phase boundary layer on the liquid injector tube outer wall is a point of extensive discussion in the literature. A detailed examination of either was beyond the scope of the present work.

Following the second subregion characterized by the three-dimensional surface structure, the jet liquid core breaks up into

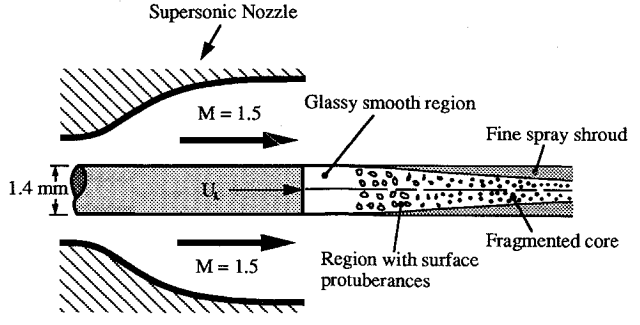

Fig. 6 Schematic diagram of the primary breakup region showing the different subregions.

large drops forming the third subregion that may be described as a fragmented core. Enveloping the fragmented core is a region of fine droplets that we term the fine-spray shroud, schematically shown in Fig. 6. The spray assumes the white, powdery appearance (Fig. 4) because of the fine-spray shroud. This fine-spray shroud was more clearly visible at a higher Mach number of 2.5 under direct observation of the jet. It is known that, in pressure atomizers under favorable conditions, the droplets at the outer edges of the spray in the primary breakup region are much smaller than the injector diameter. This is sometimes referred to in literature as the atomization regime.[28,29] Here we attempt to explain the formation of the micromist shroud by means of the boundary-layer stripping mechanism. It was originally proposed for the breakup of a large drop into fine drops when exposed to a convective gas flow. According to this, the boundary layer that develops on the drop surface by the convective gas flow is stripped away at the drop equator as a ring that further breaks up into smaller droplets. The boundary-layer stripping mechanism proposed in the present work differs from that of Refs. 6 and 13 in two important aspects. First, from a geometric aspect, boundary-layer stripping in the primary region takes place at the surface of the round liquid column as it emerges from the injector tube before the jet breaks up into large drops. Second, stripping is observed only after the development of the three-dimensional structure on the liquid surface, a fact not discussed in the earlier works.[6,13] Thus, the stripped liquid does not assume a ring shape before it breaks up into fine droplets; rather, the three-dimensional structure is stripped away directly as fine droplets. These observations are possible from the present results because of the high resolution of the photographs. A phenomenological analysis of the boundary-layer stripping mechanism was done to obtain the minimum diameter of the drops stripped off from the liquid surface. Details of the analysis are given later along with the quantitative data on drop size obtained from the P/DPA.

Drop Size Data

The P/DPA was used to acquire mean drop size, size distribution, drop velocity, and drop turbulence data. The origin of the coordinates x and r, used to represent the P/DPA data, is located at the intersection of the injector exit plane and the injector axis as shown in Figs. 1 and 2. Radial profiles at four axial locations—102, 127, 152, and 190 mm—and axial variations were obtained to quantify the spray behavior. The choice of the locations for the droplet measurements was dictated by the limitations of the instrument. Signal-to-noise ratio and data acceptance rate were too low for distances less than 100 mm (4 in.) from the nozzle exit. Reasons for the low signal-to-noise ratio are usually attributed to the presence of nonspherical drops and multiple particles in the P/DPA probe volume. Because the P/DPA works on the principle of light scattering by spherical particles, signals from nonspherical particles will be rejected by the instrument that introduces a bias in the measurements. To ensure that most of the drops were spherical at the locations selected for the P/DPA measurements, flow visualization using an 8-ns pulsed laser was performed by making axial and transverse cuts of the spray and examining the shape of the droplets in the photographs. It was confirmed that the droplets were highly spherical at the measurement locations. Therefore, the bias introduced due to the rejection of nonspherical droplets is expected to be small in the present experiments. The high drop population, on the other hand, may be causing most of the data rejection in the near field. An analytical probe volume correction[30] was applied to the drop size data to correct for the bias present when drops of different sizes traverse the edge of the probe volume. Data acceptance rate varied from 70 to 98% depending on the experimental conditions and the location of the probe volume in relation to the spray geometry. Acceptance rates were the highest at low air stagnation pressures, low liquid injection rates, and large distances from the injector exit.

The spray was checked for axial symmetry by making measurements, in a few selected cases, across the entire spray, and no significant asymmetry was noticed. The remaining measurements were, therefore, made from the axis to the edge of the spray. A few measurements were repeated on different days to check for experiment repeatability, and it was found that the Sauter mean diameter (SMD) variation was less than 1 μm in these runs. Phase errors among the three different detectors at high signal frequencies (i.e., high drop velocities) were minimized using a pulsed diode calibration system.[30]

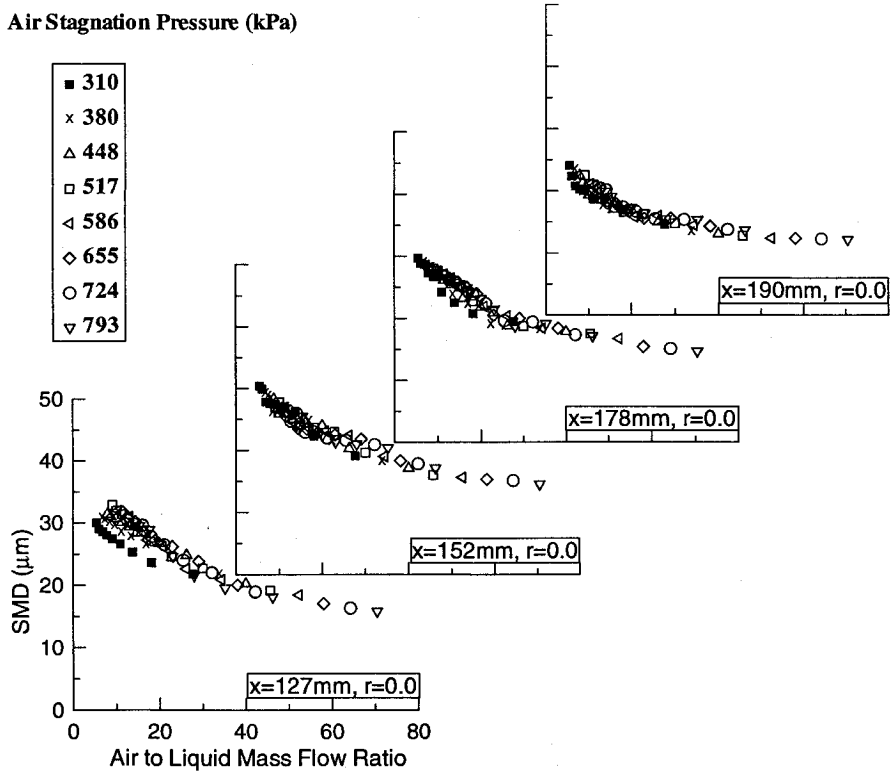

Fig. 7 SMD vs $\dot{m}_g/\dot{m}_l$ along the spray axis at four axial stations with the air stagnation pressure as the parameter.

Quantitative spray data from the P/DPA are presented in Figs. 7 and 8. The SMD vs air-to-liquid mass flow ratio $\dot{m}_g/\dot{m}_l$ is plotted in Fig. 7. The SMD is defined as

$$D_{32} = \frac{\int_0^\infty n(D)\, D^3 \mathrm{d}D}{\int_0^\infty n(D)\, D^2 \mathrm{d}D} \tag{1}$$

in which $n(D)$ represents the number density corresponding to geometric diameter D. The SMD is considered the most appropriate to express drop size since it is most relevant to rates of evaporation and combustion. A few general observations can be made based on the data presented in these figures. In Fig. 7, the air stagnation pressure was varied parametrically, and therefore each curve represents one value of stagnation pressure. The air-to-liquid mass flow ratio $\dot{m}_g/\dot{m}_l$ was varied by varying the liquid flow rate using a pressure regulator in the pressurized liquid tank. In interpreting these data, it is useful to remember that $p_0 < 370$ kPa corresponds to overexpanded operation. The SMD lies in the range 10–35 μm for the cases tested in this study. It is useful to compare these values with a typical drop-size range of 25–120 μm observed in conventional diesel sprays. The SMD variations in Fig. 7 indicate that the change in $\dot{m}_g/\dot{m}_l$ has a greater effect on SMD at lower values of $\dot{m}_g/\dot{m}_l$. As $\dot{m}_g/\dot{m}_l$ increases, the slopes of the curves become less significant. Increasing the air pressure increases the air density, whereas the velocity and the temperature remain the same. Therefore, Fig. 7 can also be thought of as showing the effect of density ratio, where each value of the air stagnation pressure corresponds to one value of the density ratio ρ_g/ρ_l. This trend is in agreement with previous works.[12,28] Except for the station closest to the jet exit (x = 127 mm), the data seem to collapse more or less into a single curve. All of the four stations shown in Fig. 7 have the same trend except for a slight reduction in data scatter with increasing downstream distance. Between the first and the last measurement stations, the SMD shows little change with increasing distance, indicating that atomization has been completed before the first measurement station and neither evaporation nor coalescence is important in the range of downstream stations shown in this figure. However, note that the experimental conditions of the present study are quite different from those that would be present in a real engine. As discussed earlier, the gas at the nozzle exit is at a very low temperature (~200 K). The liquid gets cooled by the gas during its passage through the injector. Furthermore, the droplets themselves may be cooled by the surrounding gas. Thus, the droplets can be expected to be at a very low temperature that would prevent any significant evaporation. In contrast, the gas in a jet engine is likely to raise the temperature of the droplets, promoting evaporation.

It is unlikely that freezing occurred before jet breakup in the present set of experiments since nonspherical drops were not detected in the flow visualization photographs. Drops assume their spherical shape because of surface tension; therefore, breakup after solidification would yield nonspherical shapes. For these reasons, the effect of the present lower temperatures can largely be expected to be on the rate of evaporation of the spray. More experiments using heated gas and different liquids having different freezing points are needed to fully understand the effects of solid-liquid phase change. For water, both the dynamic viscosity and the surface tension decrease (43 and 3.7%, respectively, between 0 and 20°C) as temperature increases. Variations of viscosity and surface tension with temperature are not taken into account in the present discussion.

Phenomenological Analysis of Boundary-Layer Stripping

Boundary-layer stripping was proposed in an earlier section as a mechanism that causes atomization in the primary breakup region. The following phenomenological analysis can be used to compare the measured and the estimated drop sizes. The minimum size of the drops stripped from the boundary layer may be estimated by considering the relevant forces under which boundary-layer stripping takes place. The three-dimensional protuberances (Figs. 4 and 6) that grow on the liquid jet surface will be acted upon by the surface shear force and the opposing surface tension force. When the shear force becomes equal to the surface tension force, the protuberance will be stripped away from the surface as a droplet. The droplet diameter can be estimated by equating these two forces as given next:

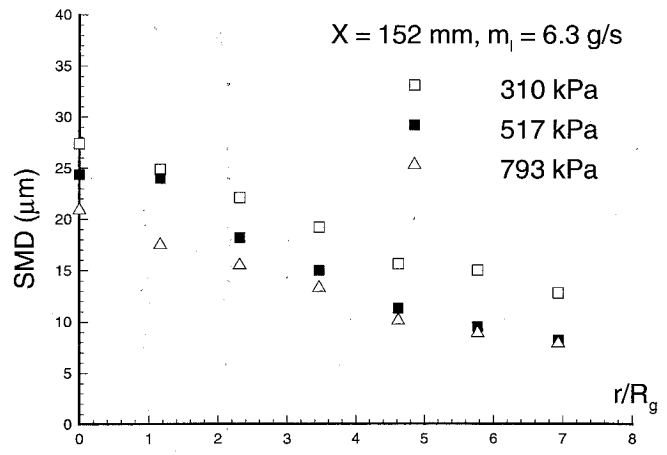

Fig. 8 Radial profiles of SMD at x = 152 mm for $\dot{m}_l$ = 6.3 g/s. Air stagnation pressure is the parameter.

$$\frac{c_f \rho_g U_g^2 S}{2} = l\sigma \tag{2}$$

At the injector exit, the gas velocity U_g is much higher than the liquid velocity U_l. Therefore, the relationship $U_g - U_l \approx U_g$ can be assumed, which justifies the use of U_g for calculating the aerodynamic Weber number in this analysis. To estimate the minimum diameter of the droplets that will be stripped away, a few assumptions must be made. If one assumes the protuberance to be hemispherical, S and l can be expressed in terms of the base diameter of the protuberance. Substitution in Eq. (2) will yield the following expression for the base diameter:

$$d = \frac{4\sigma}{c_f \rho_g U_g^2} \tag{3}$$

A numerical value for d can be obtained if c_f is known. For large values of the roughness factor, the skin friction coefficient c_f in Eq. (2) becomes nearly independent of the Reynolds number.[26] A reasonable estimate of c_f can be made by assuming it to be the same as that of a fully rough flat plate that yields, after applying a compressibility correction factor, an approximate value of 0.0196.[26] The minimum drop size thus calculated for an airstream dynamic pressure of 159 kPa (p_0 = 380 kPa, abs) equals 56 μm, which compares well with the drop size measured at the outer edges of our spray. A similar calculation for the coaxial jet in subsonic flow[23] using a value of c_f = 0.02, which differs from the value used in our compressible flow case because of the compressibility correction factor, yields a drop size of 6 mm. Obviously, the conclusion in Ref. 23 that skin friction drag did not contribute to jet breakup is consistent with the preceding size estimates of drops stripped away from the boundary layer. One can thus conclude that boundary-layer stripping would probably be limited to cases in which the gas phase dynamic pressure is large such as in the present experiments and those in Ref. 6. It may be noted from Eq. (2) that the nondimensional parameter relevant to boundary-layer stripping is the aerodynamic Weber number based on the gas phase dynamic pressure and the base diameter of the protuberance.

Representative radial profiles of SMD are plotted in Fig. 8 with the air stagnation pressure as the parameter for the axial station x = 152 mm and $\dot{m}_l$ = 6.3 g/s. For these cases as well as cases for other values of and $\dot{m}_l$ and x not shown, the drops are smaller toward the outer edges of the spray. This is in contrast to the trend recently reported[11] in a similar work on a slit atomizer, in which the SMD increased toward the outer edges of the spray. This trend can be attrib-

uted to the low values of $\dot{m}_g/\dot{m}_l$ and the angle between the air jet and the liquid jet used in that work. It is quite possible that some of the large drops formed by the primary breakup might have escaped to the quiescent ambient air preventing further breakup. Moreover, boundary-layer stripping in the primary region might have been prevented by the oblique impact of the air jet on the liquid jet and the subsequent shattering of the liquid jet into large drops before fine drops could be stripped away from the liquid column.

IV. Conclusion

The present study provides valuable insight into the atomization of a round liquid jet when injected into a coaxial, coflowing, Mach 1.5 flow. It is shown that the shape of the spray boundary in the primary atomization region can be explained by means of the principles of a supersonic jet interacting with a constant pressure boundary. In particular, the formation of a bubblelike region that causes the eventual breakup of the liquid into a fine spray is described. The following specific observations may be made regarding the gross behavior of the spray:

1) There is strong interaction between the supersonic wave structure and the liquid jet that may be contributing to the disintegration of the liquid jet into fine droplets.

2) The initial shape of the spray boundary is controlled by the pressure distribution resulting from the shock and expansion waves generated by the supersonic flow around the liquid jet.

3) Higher liquid-to-gas pressure ratio (p_{el}/p_{eg}) resulted in higher initial spray angles.

In closeup, the following processes seem to be associated with the primary evolution of the spray: formation of the three-dimensional structure on the liquid surface, followed by boundary-layer stripping of the structure into fine droplets, and a dramatic enlargement of the spray cross section upon interaction with the supersonic wave structure causing further disintegration of the liquid core. The dynamic pressure of the gas phase appears to influence the three-dimensional structure on the liquid surface. It is believed that the drops in the fine-spray shroud observed in the experiments may have sizes dependent on this surface structure. A Weber number based on the gas phase dynamic pressure and the base diameter of the protuberances that grow on the liquid jet surface has been identified, using a phenomenological analysis, as the nondimensional parameter relevant to boundary-layer stripping. Valuable, but not exhaustive, drop size data from a P/PDA are presented. The decreasing drop size in the radial direction shows a significant departure from the results of an earlier study by other workers on a two-dimensional atomizer using a slit injector, in which the droplet diameter increased toward the edge of the spray.

The objective of this study was to establish the overall characteristics of the spray. Effects of viscosity and surface tension, interaction of the gas boundary layer with the liquid jet, etc., are some of the important areas that need to be investigated in future work. Detailed mapping of the spray will help to establish correlations.

Acknowledgments

This work was done at the University of Missouri—Rolla Aeropropulsion Laboratory established with partial funding from the James F. McDonnell Foundation and the university's Center for Advanced Technology. We thank C.-Y. Wei for his contributions as a member of our team and the department technicians for their help and support rendered during this effort.

References

[1]Law, C. K., "Recent Advances in Droplet Vaporization and Combustion," *Progress in Energy and Combustion Science*, Vol. 8, No. 3, 1982, pp. 171–201.

[2]Mayer, E., "Theory of Liquid Atomization in High Velocity Gas Streams," *ARS Journal*, Vol. 31, No. 12, 1961, pp. 1783–1785.

[3]Sherman, A., and Schetz, J. A., "Breakup of Liquid Sheets and Jets in Supersonic Gas Stream," *AIAA Journal*, Vol. 9, No. 4, 1971, pp. 666–673.

[4]Nejad, A. S., and Schetz, J. A., "Effect of Properties and Location in the Plume on Droplet Diameter for Injection in a Supersonic Stream," *AIAA Journal*, Vol. 21, No. 7, 1983, pp. 956–961.

[5]Hermanson, J. C., Papas, P., and Kay, I. W., "Structure and Penetration of a Transverse Fluid Jet Injected at Supercritical Pressure into Supersonic Flow," AIAA Paper 92-3652, July 1992.

[6]Ranger, A. A., and Nicholls, J. A., "Aerodynamic Shattering of Liquid Drops," *AIAA Journal*, Vol. 7, No. 2, pp. 285–290.

[7]Eastes, T. W., and Samuelson, G. S., "Secondary Atomization by High Amplitude Pressure Waves," AIAA Paper 92-3120, July 1992.

[8]Weiss, M. A., and Worsham, C. H., "Atomization in High Velocity Air Streams," *ARS Journal*, Vol. 29, No. 4, 1959, pp. 252–259.

[9]Farago, Z., and Chigier, N., "Morphological Classification of Disintegration of Round Liquid Jet in a Coaxial Air Stream," *Atomization and Sprays*, Vol. 2, No. 2, 1992, pp. 137–153.

[10]Mayer, W., and Krulle, G., "Rocket Engine Coaxial Injector Liquid/Gas Interface Flow Phenomena," AIAA Paper 92-3389, July 1992.

[11]Kihm, K. D., and Chigier, N., "Effect of Shock Waves on Liquid Atomization of a Two-Dimensional Atomizer," *Atomization and Sprays*, Vol. 1, 1991, pp. 113–136.

[12]Reitz, R. D., and Bracco, F. V., "Mechanism of Atomization of a Liquid Jet," *Physics of Fluids*, Vol. 25, No. 10, 1982, pp. 1730–1742.

[13]Taylor, G. I., "The Shape and Acceleration of a Drop in a High Speed Air Stream," *The Scientific Papers of G. I. Taylor*, edited by G. K. Batchelor, Vol. III, University Press, Cambridge, England, UK, 1963, pp. 457–464.

[14]Wei, C.-Y., Drallmeier, J. A., and Isaac, K. M., "Analysis of Primary Atomization in Supersonic Coaxial Systems," AIAA Paper 92-3236, July 1992.

[15]Missoum, A., Isaac, K. M., and Drallmeier, J. A., "Atomization of Liquid Fuels in Supersonic Flow," AIAA Paper 92-3235, July 1992.

[16]Bachalo, W. D., and Houser, M. J., "Phase/Doppler Spray Analyzer for Simultaneous Measurements of Drop Size and Velocity Distributions," *Optical Engineering*, Vol. 23, No. 9, 1984, pp. 583–590.

[17]Love, E. S., Grigsby, C. E., Lee, L. P., and Wooding, M. J., "Experimental and Theoretical Studies of Axisymmetric Free Jets," NASA TR-R6, 1959.

[18]Oswatitsch, K., *Gasdynamik*, Springer, Vienna, 1952; see also Academic Press, New York, 1956, Chap. 8.

[19]Liepmann, H. W., and Roshko, A., *Elements of Gas Dynamics*, Wiley, New York, 1957, Chap. 4.

[20]Courant, R., and Friedrichs, K. O., *Supersonic Flow and Shock Waves*, Interscience, New York, 1948, Chap. 5.

[21]Brennen, C., "Cavity Surface Wave Pattern and General Appearance," *Journal of Fluid Mechanics*, Vol. 44, Pt. 1, 1970, pp. 33–49.

[22]Hoyt, J. W., and Taylor, J. J., "Turbulent Structure in a Water Jet Discharging in Air," *Physics of Fluids*, Vol. 20, No. 10, Pt. II, 1977, pp. S253–S257.

[23]Hoyt, J. W., and Taylor, J. J., "Waves on Water Jets," *Journal of Fluid Mechanics*, Vol. 83, Pt. 1, 1977, pp. 119–127.

[24]Van Dyke, M., *An Album of Fluid Motion*, Parabolic Press, Stanford, CA, 1982, Chap. 5.

[25]Panton, R. L., *Incompressible Flow*, Wiley, New York, 1984, Chap. 22.

[26]White, F. M., *Viscous Fluid Flow*, 2nd ed., McGraw-Hill, New York, 1990, Chap. 6.

[27]Roshko, A., private communication, Memphis, TN, Oct. 1991.

[28]Faeth, G. M., "Structure and Atomization Properties of Dense Turbulent Sprays," *Twenty-third Symposium (International) on Combustion*, Combustion Inst., Pittsburgh, PA, 1990, pp. 1345–1352.

[29]Wu, P. K., and Faeth, G. M., "Aerodynamic Effects of Primary Breakup of Turbulent Liquids," *Atomization and Sprays*, Vol. 3, No. 3, 1993, pp. 265–289.

[30]Anon., "Aerometrics Doppler Signal Analyzer for Phase Doppler Particle Sizing Applications User's Manual," Aerometrics, Inc. Report, Sunnyvale, CA, 1992.